5.1 Introduction

In this chapter, cobalt substitution has been optimized in $SrAl_4Fe_8O_{19}$ hexaferrite. It is reported that partial substitution of Co can improve the magnetic properties, especially enhancement in the magnetization [Gordania *et al*. (2014)]. Since, it is famed for giving a strong contribution to the remanence (*Br*) in the magnetic properties. So, this substitution of cation at Fe sites may be an effective method to vary the physical, magnetic and electrical properties of strontium hexaferrite.

In this work, investigation has been made to explore the effect of the Co substitution in $SrAl_4Fe_8O_{19}$. Successfully synthesized the Co substituted $SrAl_4Fe_{8-x}Co_xO_{19}$ ferrites (where, x = 0, 0.2, 0.4, 0.6, 0.8, & 1) by sol-gel auto combustion, as explained in section 3.1.1. The phase, microstructure evolution, magnetic, dielectric, and electrical properties of the ferrites have been investigated. Structural parameters are explored and followed out by Rietveld refinement. Magnetic parameters are measured at room temperature with a maximum magnetic field of 70 kOe. The variation in the dielectric constant and resistivity are discussed in the frequency range of 20 Hz–20 MHz.

5.2 Results and Discussion

Figure 5.1 shows the FTIR spectra of calcined $SrAl_4Co_xFe_{8-x}O_{19}$ (x = 0.0, 0.2, 0.4, 0.6, 0.8, & 1.0) ferrite powders in the frequency range from 4000 to 400 cm^{-1}. This spectra shows the major peaks at about 1468 cm^{-1}, 629 cm^{-1}, 576 cm^{-1}, and 468 cm^{-1}. All compositions have been exhibited the peaks at about 629 cm^{-1}, 576 cm^{-1}, and 468 cm^{-1} in the area between 400 cm^{-1} to 800 cm^{-1} in every curve. It is attributed to the vibrations of metal ion–oxygen complexes in the tetrahedral (ν_1) and octahedral (ν_2) sites, respectively. It is indicated that the $SrFe_{12}O_{19}$ phase is formed. Ferrite bands occur due to tetrahedral and octahedral complexes.

The bands are assigned to the vibration of ions present in the crystal lattices, caused by the tetrahedral and octahedral Fe^{+3}–O^{-2} distances. The peak at 1468 cm^{-1} signifies to the stretching vibration of Co-O-Co bond [Kaur *et al*. (2017)].

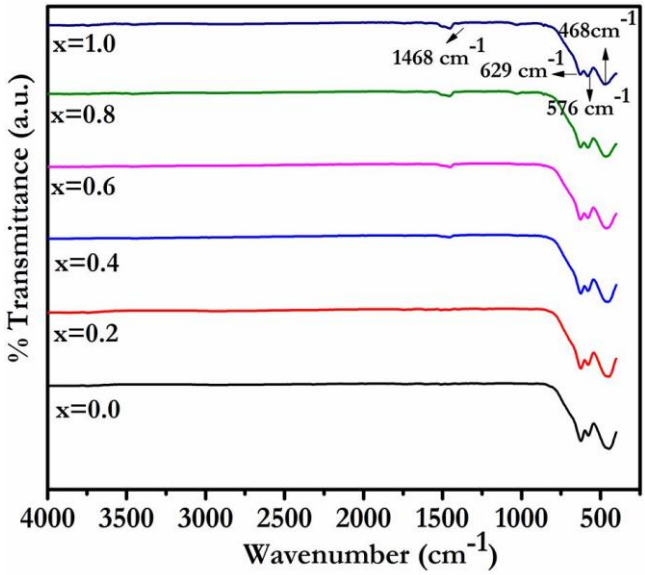

Figure 5.1 FTIR spectra of $SrAl_4Co_xFe_{8-x}O_{19}$ ferrite with different Co contents.

Figure 5.2 shows the XRD patterns for sintered $SrAl_4Fe_{8-x}Co_xO_{19}$ (x = 0.0, 0.2, 0.4, 0.6, 0.8, & 1.0) ferrite samples. From XRD patterns, it can be seen that all the reflections are belonging to the single phase M-type strontium ferrite (JCPDS No. 720739) [Debnath *et al*. (2015)] with no other impurity phases. This means that Co^{+2}, Al^{+3} ions have been dissolved in the hexagonal structure properly to fulfill the formation of a single phase Sr ferrite. Liu *et al*. (2012) and Wang *et al*. (2012) also have been reported the formation of single phase strontium hexaferrite with the substitution of Co and Al at high temperature without any secondary phase.

Structural parameters are further studied through Rietveld refinement, as discussed in section 3.4.3 by using *P63/mmc* space group [Kupferling *et al*. (2006)]. Rietveld refinement

of the XRD patterns of $SrAl_4Fe_8O_{19}$ and $SrAl_4Co_{1.0}Fe_7O_{19}$ are manifested in Figure 5.3. The refined parameters, i.e., R_p, R_{wp} and χ^2, lattice parameters, crystallite size, and *c/a* ratio of the sintered samples are included in Table 5.1. The credibility of the refinement is estimated by the low values of R_p, R_{wp} and goodness of fit (χ^2).

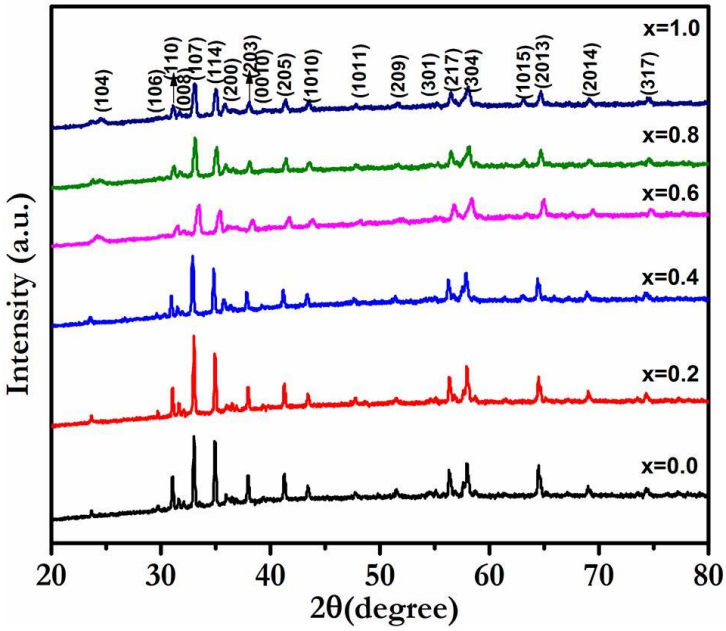

Figure 5.2 XRD pattern of sintered $SrAl_4Co_xFe_{8-x}O_{19}$ ferrite with different Co contents.

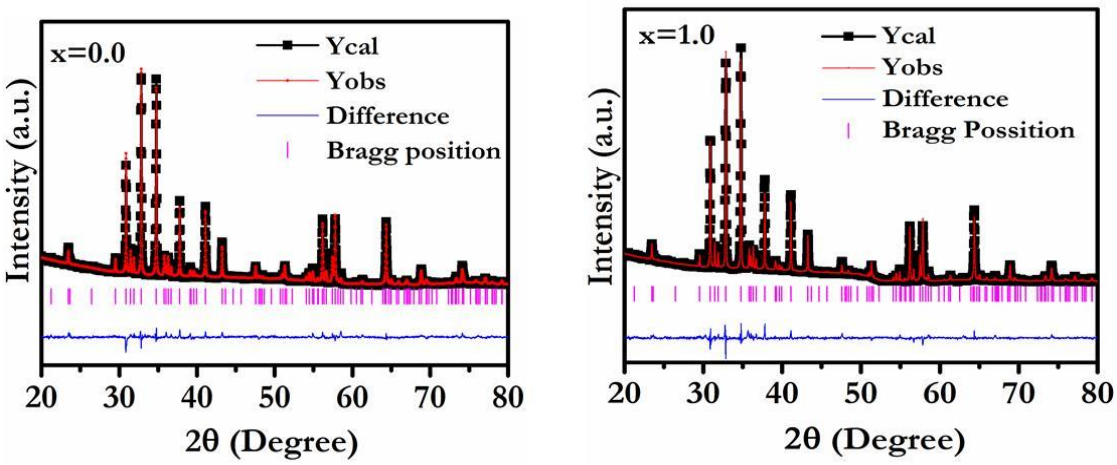

Figure 5.3 Rietveld refinement of sintered x = 0.0; $SrAl_4Fe_8O_{19}$ and x = 1.0;

$SrAl_4Co_1Fe_7O_{19}$ferrites.

Table 5.1 Reliable factors (R_p, R_{wp} and χ^2), lattice parameter, crystallite size and *c/a* ratio of sintered $SrAl_4Co_xFe_{8-x}O_{19}$ samples.

Composition (x)	**R_p (%)**	**R_{wp} (%)**	**χ^2**	**Lattice parameter (Å)**		**Crystallite size (nm)**	***c*/*a***
				(a)	***(c)***		
0	2.06	2.65	1.65	5.78	22.72	12.64	3.93
0.2	2.57	3.59	2.13	5.78	22.69	12.51	3.92
0.4	2.81	5.57	2.74	5.78	22.65	12.32	3.91
0.6	2.51	3.37	2.49	5.77	22.64	12.01	3.92
0.8	2.67	3.78	2.02	5.77	22.61	11.96	3.91
1.0	3.01	4.13	2.34	5.76	22.62	12.16	3.92

It exhibits constant parameter *a* and variable parameter *c* with the different Co content. This indicates that the change of the main axis (*c*-axis) is greater than that of *a*-axis for the substitution of Co ion. "*c*" slightly decreases with the increasing concentration of Co. It may be due to the results from the difference in ionic radii of Co^{+2} (0.63Å) and Fe^{+3} ion (0.67Å). The smaller ion replacing Fe^{+3} ion leads to lattice contraction of the unit cell. Crystallite size has been calculated by using Debye-Scherrer's formula with Caglioti equation. It has also been observed that crystallite size decreases with Co content. This supports the fact that Co^{+2} ions simply replace the Fe^{+3} ions, without distorting the hexagonal lattice structure. This decrease in the crystallite size of $SrAl_4Co_xFe_{8-x}O_{19}$ with Co^{+2} addition may be associated with the decrease in the lattice constant as well. A slight increase in crystallite size for x = 1.0 composition may be due to the increasing strain in the sample. An important factor, which

validates the M-type structure is the *c*/*a* ratio and this ratio is smaller than 3.98 for the magnetoplumbites. The estimated *c*/*a* parameters in this study is less than 3.98, it confirms the formation of the magnetoplumbite structure in the present matrix [Zhang *et al*. (2012)].

Table 5.2 Bulk density, grain size and elemental composition of sintered $SrAl_4Co_xFe_{8-x}O_{19}$ ferrites with ($0 \leq x \leq 1.0$).

Composition (x)	Density (g/cm^3)	Grain Size (μm)	Elemental composition (At%)			
			Sr	Al	Co	Fe
0.0	5.08	1.11	3.07	14.09	-	34.31
0.2	5.15	1.70	3.01	14.03	0.15	30.89
0.4	5.41	1.73	3.17	14.01	0.28	27.58
0.6	5.67	1.76	3.02	13.85	0.45	23.79
0.8	5.90	1.79	3.14	13.81	0.61	20.19
1.0	5.86	1.75	3.16	13.96	0.86	19.32

Table 5.2 shows the bulk density, grain size, and elemental composition of the sintered $SrAl_4Co_xFe_{8-x}O_{19}$ ferrites. It is showing that a significant increase in the bulk density of the sintered samples with the substitution of Co ions up to x = 0.8. Cobalt helps for densification and reduces the liquid formation temperature in ceramics [Byun *et al*. (1999), Tabrizi and Nassaj (2010), Schmitt and Raether (2014)]. Increment in density may be due to the heavier densed atom [Co (8.90 g/cm^3)] substitutes the lower densed [Fe (7.87 g/cm^3)] atom. While at x = 1.0, density is decreased. Bhuvaneswari *et al.* (2016) have reported that excess amount of Co^{+2} content creates the compressive strain in the system. It induces the

defect density in the system and confines the grain growth by dropping down the grain size, as shown in Table 5.2.

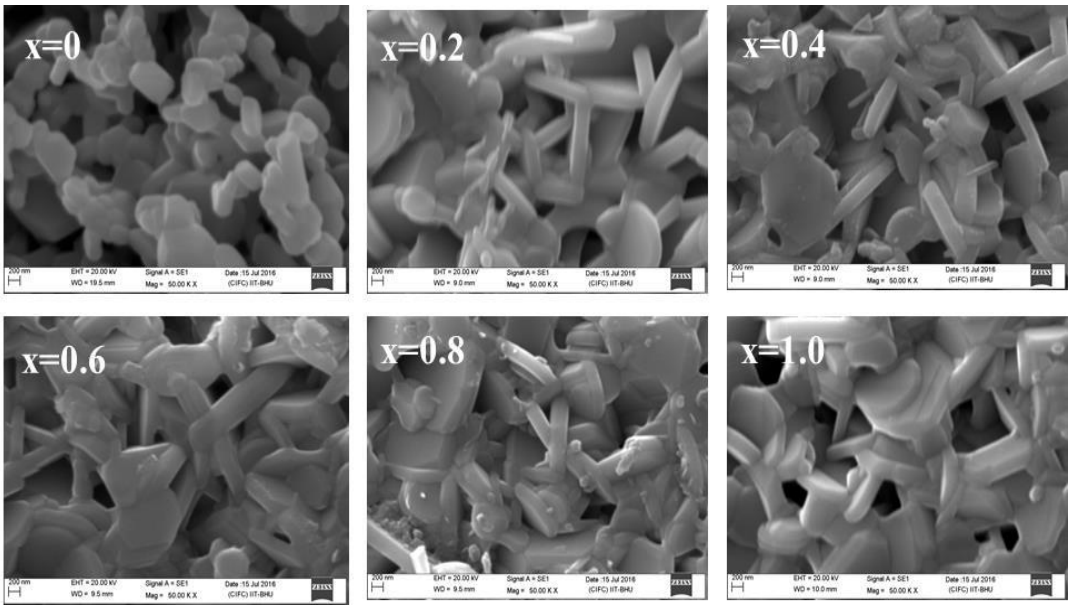

Figure 5.4. SEM micrograph of sintered $SrAl_4Co_xFe_{8-x}O_{19}$ samples.

Microstructure plays a key role in obtaining the desired dielectric and magnetic properties of these materials. Figure 5.4 shows the microstructure and morphology of the ferrite sample, obtained from SEM images. The samples exhibit relatively well defined, nearly hexagonal grains and the surface of the grain seems to be more compacted. It is composed of needle like shaped and platelet particles. The average grain sizes are tabulated in Table 5.2. The average grain size increases with the increase in cobalt content up to x = 0.8. This suggests that Co substitution tends to encourage the grain growth. This increase in grain size can also be the reason for continuous reduction in H_C (Table 5.3). With an increase in grain size, grain boundaries decrease causing a reduction in pinning sites for spins and hence a drop in coercivity. While at x = 1.0, grain size is decreased. This decrease in grain is happened due to too much Co^{+2} content increased in the system. Higher cobalt content

induces the compressive strain, results decrease in grain size [Bhuvaneswari *et al.* (2016)]. Elemental analysis has been performed through EDX of the sintered $SrAl_4Co_xFe_{8-x}O_{19}$ hexaferrite, as shown in Figure 5.5. Atomic percentage (At %) of Sr, Al, Co, and Fe in hexaferrites are listed in Table 5.2. It indicates that single phase SrM has been formed without any impurity. At % of Co increases and Fe is decreased with substitution in the structure.

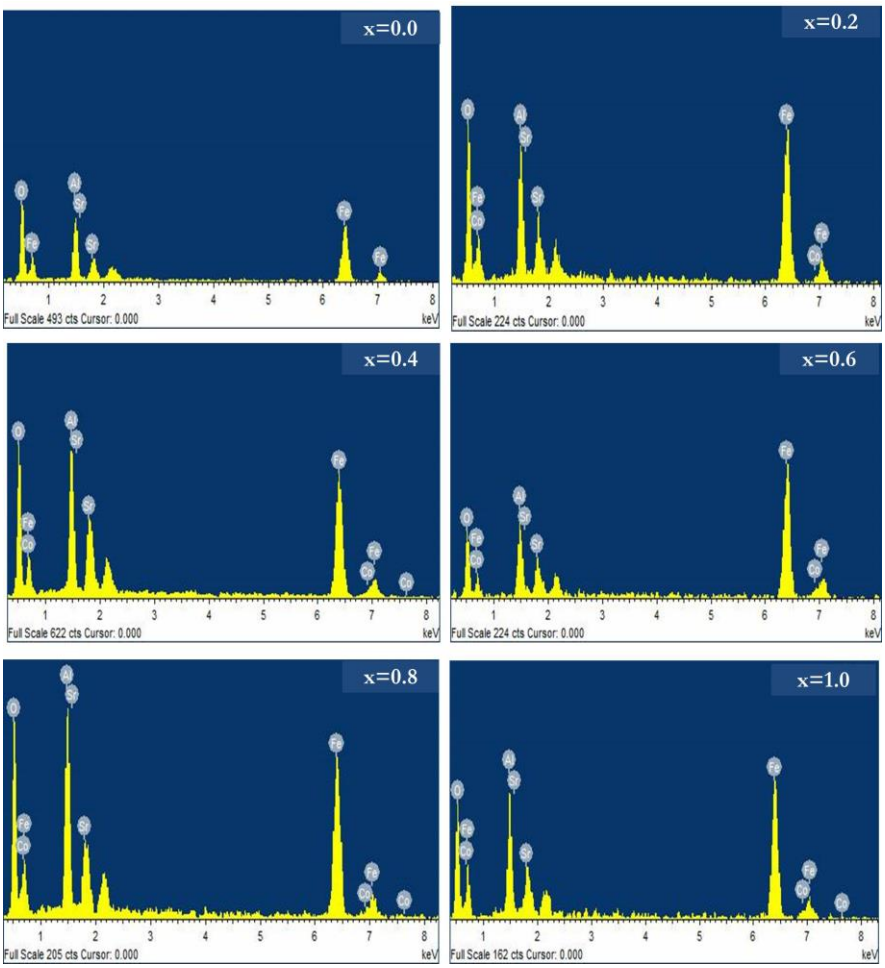

Figure 5.5. EDX spectra of sintered $SrAl_4Co_xFe_{8-x}O_{19}$ samples.

Figure 5.6 to Figure 5.10 demonstrates the magnetic behavior of Co substituted ,i.e., $SrAl_4Fe_{8-x}Co_xO_{19}$ (x = 0.0, 0.2, 0.4, 0.6, 0.8, & 1.0) hexaferrites at room temperature.

Figure 5.6 illustrates the *M–H* loops of $SrAl_4Fe_{8-x}Co_xO_{19}$ ($0 \leq x \leq 1.0$) hexaferrites. Hysteresis curve is demonstrating that M_s continuously increases and H_c decreases with the substitution.

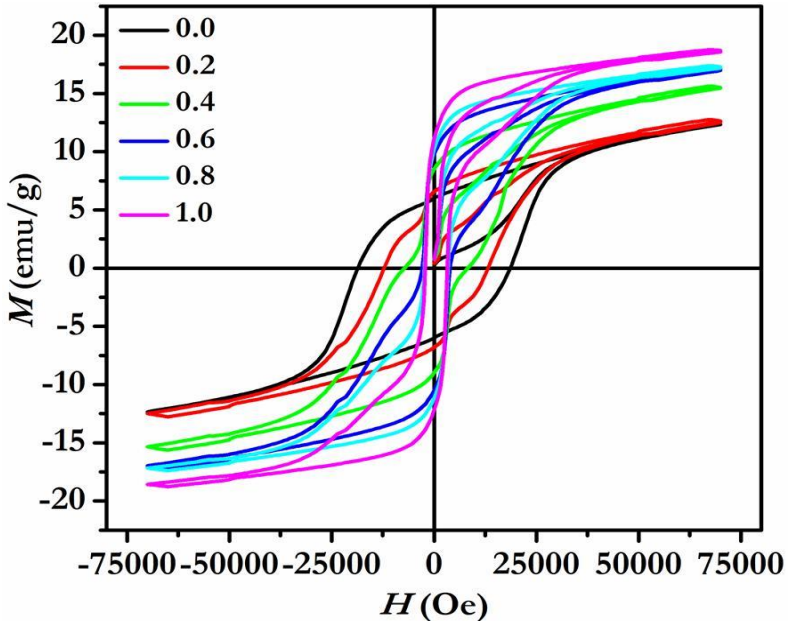

Figure 5.6 Room temperature hysteresis loop of $SrAl_4Fe_{8-x}Co_xO_{19}$ ferrite with different Co contents.

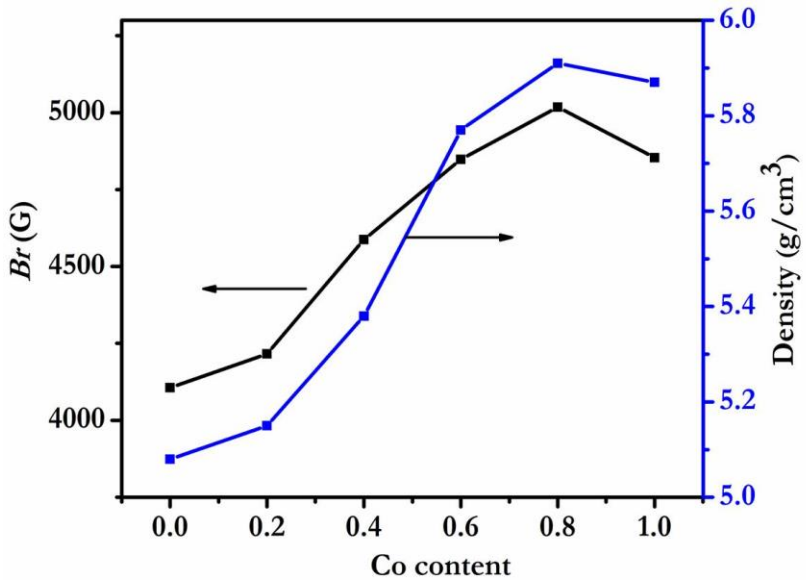

Figure 5.7 Variation of *Br* and bulk density with function of Co content in $SrAl_4Co_xFe_{8-x}O_{19}$ hexaferrites.

Table 5.3 Magnetic parameters *Br*, μ_B, iH_c, bH_c, H_k/iHc, $(BH)_{max}$, k_{eff}, and Tc of sintered $SrAl_4Co_xFe_{8-x}O_{19}$ ferrites with ($0 \leq x \leq 1.0$).

Composition (x)	***Br*** **(kG)**	μ_B	iH_c **(kOe)**	bH_c **(kOe)**	H_k/iHc	$(BH)_{max}$ **(MGOe)**	$k_{eff\ x10^6}$ **(erg/cm^3)**	**Tc (ºC)**
0.0	4. 10	4.02	18.15	18.02	0.89	6.03	3.54	320
0.2	4.21	4.15	10.91	10.14	0.90	5.54	2.90	227
0.4	4.58	4.63	5.73	5.10	0.91	4.96	2.67	218
0.6	4.84	4.96	1.39	1.02	0.93	4.35	2.31	216
0.8	5.01	5.19	0.86	0.62	0.95	3.68	2.29	203
1.0	4.85	4.90	0.73	0.56	0.88	3.26	2.01	201

Flux density (*B*) is calculated by using the equation 3.16. Figure 5.7 shows the variation of *Br* with bulk density as a function of Co substitution. Table 5.3 shows the magnetic parameters of sintered $SrAl_4Co_xFe_{8-x}O_{19}$ ferrites with ($0 \leq x \leq 1.0$). *Br* is mostly depends on the magnetization (M_s) of the material. The values of magnetization increases with Co substitution up to x = 0.8, further it decreases at x = 1.0 substitution. Magnetic properties of the materials are strongly affected by the substitution of cations on different crystallographic sites. In this study, increasing the magnetization values can be explained by the site preference of Co^{+2} ions at low concentrations in the $4f_1$ and $4f_2$ sub-lattice of Fe^{+3} ions. This in turn decreases the negative magnetic moment of Fe^{+3} and thereby enhances M_s. The magnetic moment is calculated by using the equation 3.23. It is increased up to x = 0.8, then it is decreased at x = 1.0 composition. The magnetic moment of Co^{+2} (3 μ_B) is lower than that of Fe^{+3} (5 μ_B), so substitution of Fe^{+3} from the $4f_2$ site by Co^{+2} may increase M_s of the samples [Pieper *et al*. (2002)]. Actually, the occupation of Co^{+2} in $4f_2$ sites decreases magnetic moment

in the opposite direction, and slightly increases the magnetic moment. This is the reason that magnetization of the magnets increases with the increase of dopant contents. It is well established that saturation magnetization of polycrystalline ferrite increases with increasing bulk density and grain size. Increase in M_s with Co substitution may primarily be attributed to the increase in bulk density. An increase in the density, not only results in the reduction of demagnetizing field due to the reduction of pores, but also raises the spin rotational contribution, which in turn increase the saturation magnetization [Shrotri *et al*. (1999)]. At x = 1.0 Co substitution, magnetization is decreased. This is happened due to excess amount of Co^{+2} ions are increased in strontium hexaferrite structure. That leads to weakening the super exchange interaction between the Fe^{+3} sites [Xie *et al*. (2018)].

Table 5.4 Average Fe-O bond lengths in $SrAl_4Co_xFe_{8-x}O_{19}$ with ($0 \leq x \leq 1.0$).

Site	Bond Type	0.0 Avg.	0.2 Avg.	0.4 Avg.	0.6 Avg.	0.8 Avg.	1.0 Avg.
Fe1 (*2a*, O)	Fe-O	1.931(0)	1.912(1)	1.891(5)	1.876(1)	1.854(3)	1.897(0)
Fe2 (*2b*,TBP)	Fe-O	1.793(2)	1.743(0)	1.721(1)	1.710(0)	1.696(3)	1.741(1)
Fe3 ($4f_1$,T)	Fe-O	2.031(0)	1.978(4)	1.943(6)	1.914(2)	1.891(0)	1.901(3)
Fe4 ($4f_2$,O)	Fe-O	2.086(2)	2.051(4)	1.983(3)	1.961(2)	1.934(2)	1.985(1)
Fe5 (*12k*,O)	Fe-O	1.976(0)	1.963(1)	1.941(3)	1.925(2)	1.891(1)	1.961(0)

The super-exchange interaction exists between the magnetic ions, which are coupled with O^{-2} ions [Kaur *et al*. (2017)]. This interaction becomes weak when, the distance between the magnetic ions increases. Structural aspects tell about these interactions through bond length and bond angle between the magnetic ions. In addition, Anderson *et al*. (1963) has proposed that if the bond angle, Fe^{+3}_i - O^{-2} - Fe^{+3}_j ($1 \leq i \,\&\, j \leq 5$) is close to 180°, then

magnetic interactions may be strongest and weakest if the bond angle is near to 90°. Moreover, if bond length reaches to 3 Å distance, than the magnetic interactions may become insignificant [Anderson *et al*. (1963)]. Table 5.4 shows the average Fe-O bond lengths within the sub-lattices of the hexaferrites. Table 5.5 shows the bond angles between the sub-lattice of the system. From the Table 5.4, it is found that all the bond lengths are less than 3 Å, which shows that the interactions are significant between magnetic ions. It is also observed that the bond angles are tending to increase and bond length are finding to decrease up to x = 0.8. It designates that the interaction is increased with substitution and hence the increase in magnetization, accordingly. For x = 1.0 signifies to decrease in interactions and hence a decrease in the magnetization.

Table 5.5 Fe^{+3}_{i} - O^{-2} - Fe^{+3}_{j} ($1 \leq i \,\&\, j \leq 5$) bond angles for $SrAl_4Co_xFe_{8-x}O_{19}$ ($0 \leq x \leq 1.0$).

Bond Type	**0.0**	**0.2**	**0.4**	**0.6**	**0.8**	**1.0**
Fe1(*2a*)-O4-Fe3(*4f*$_1$)	126.513(0)	126.544(0)	129.025(1)	129.616(0)	131.131(0)	128.891(1)
Fe1(*2a*)-O4-Fe5(*12k*)	92.120(1)	92.803(0)	94.503(0)	95.317(2)	97.325(0)	96.612(0)
Fe2(*2b*)-O3-Fe4(*4f*$_2$)	135.321(0)	136.897(0)	140.854(0)	142.314(0)	145.672(1)	140.176(0)
Fe2(*2b*)-O1-Fe5(*12k*)	126.517(0)	128.678(1)	131.612(0)	135.543(0)	137.813(0)	134.391(0)
Fe3(*4f*$_1$)-O2-Fe5(*12k*)	110.011(0)	115.411(0)	121.617(0)	129.314(1)	132.189(0)	128.623(0)
Fe4(*4f*$_2$)-O5-Fe5(*12k*)	127.217(0)	128.267(2)	131.821(0)	134.912(0)	137.623(1)	135.934(0)
Fe4(*4f*$_2$)-O3-Fe4(*4f*$_2$)	95.151(1)	97.368(0)	101.211(0)	106.213(1)	110.614(0)	108.427(1)
Fe5(*12k*)-O5-Fe5(*12k*)	92.017(0)	96.371(0)	101.859(0)	107.611(0)	112.912(0)	110.345(0)
Fe5(*12k*)-O4-Fe3(*4f*$_1$)	114.416(1)	117.238(0)	120.345(1)	122.194(0)	125.658(0)	122.352(0)
Fe5(*12k*)-O2-Fe5(*12k*)	94.213(0)	97.561(0)	99.186(0)	103.025(1	105.161(0)	102.617(1)

From Figure 5.8, it is found that the coercivity (iH_c and bH_c) decreases gradually with the composition. It may be due to morphology and magneto-crystalline anisotropy (k_{eff}). The coercivity may correlate with the anisotropy (k_{eff}) and the capacity of anti-demagnetization. Generally, the iH_c decreases with the decrease of the anisotropy constant. Anisotropy constant k_{eff} is calculated as described in section 3.4.4 and Figure 5.9 shows the typical M versus $1/H^2$ curve of $SrAl_4Co_xFe_{8-x}O_{19}$ for x = 0.0 and x = 1.0.

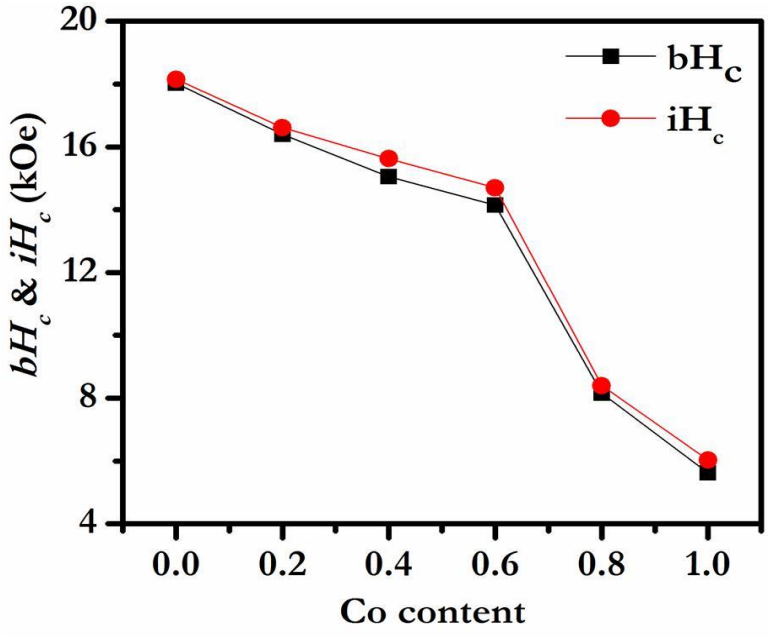

Figure 5.8 Coercivity (iH_c and bH_c) with function of the Co content.

From Table 5.3, it has been observed that k_{eff} decreases with Co content. The decrease in k_{eff} with composition may be due to the decrement in spin-orbit coupling [Kumari *et al*. (2015)]. Generally, the H_c decreases with the decrease of the anisotropy (k_{eff}) constant. It also has been reported that when the grain size increases, coercivity decreases [Singhal *et al*. (2010)]. This variation of coercivity with grain size can be explained on the basis of domain structure, critical diameter, the anisotropy of the crystal, and domain wall energy [Cullity

(1972)]. In the multi domain region, the coercivity decreases as the grain size increases [George *et al*. (2006)]. Table 5.3 shows the variation of the squarness ratio (H_k/iH_c) with Co content. Where, H_k is the knee field, which denotes the anisotropy constant (k_{eff}) of the system. From Table 5.3, it shows this ratio is >0.85, which belongs to square loop ferrite, i.e., permanent magnet. Figure 5.10 shows the energy $(BH)_{max}$ with the function of Co content. It is decreased with the substitution. The value of $(BH)_{max}$ of x = 1.0 is shown in inset Figure 5.10. It can be found that the varying trend of energy product of the ferrite is in harmony with coercivity of the synthesized hexaferrite.

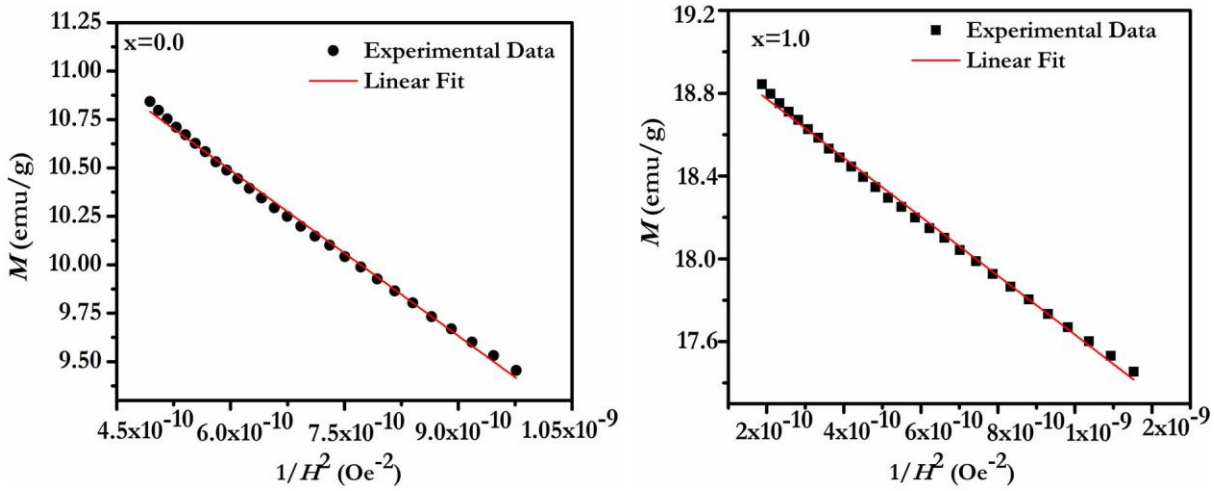

Figure 5.9 Typical *M* versus $1/H^2$ curve of $SrAl_4Co_xFe_{8-x}O_{19}$ for x = 0.0 and x = 1.0.

Table 5.3 shows the Curie temperature values of $SrAl_4Co_xFe_{8-x}O_{19}$ ferrites. It is decreased with Co substitution. Co^{+2}(~ $3\mu_B$) substitutes Fe^{+3}(~ $5\mu_B$), creates a deviation of collinear arrangement of magnetic moment that is so called spin canting structure [Liu *et al*. (2006)]. Spin canting structure that is responsible for decreasing of Tc (Curie temperature) with the substitution. The decrease of Curie temperature with substitution may be because of Fe ions is reduced as Co enters the lattice and/or due to crystalline disorder increases with substitution.

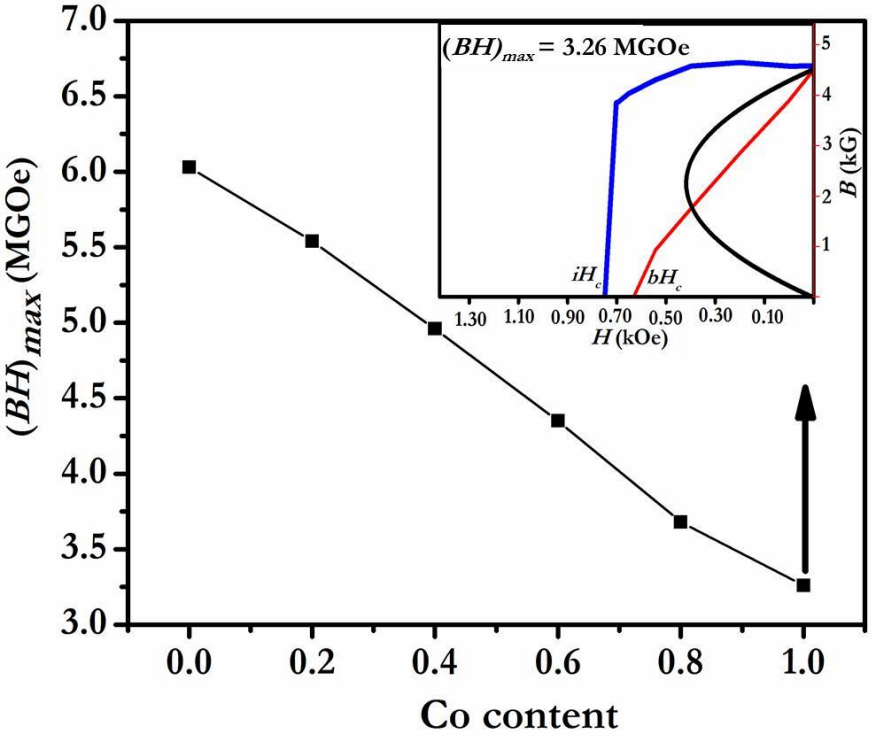

Figure 5.10 Energy product $(BH)_{max}$ with the function of Co content and typical demagnetization curve for x = 1.0 composition.

Table 5.6 Dielectric constant and resistivity of sintered $SrAl_4Co_xFe_{8-x}O_{19}$ samples.

Composition (x)	**Dielectric constant (Ɛ) at 1 MHz**	**ρ (Ω-cm) x 10^4 at 1 MHz**
0	20.52	5.54
0.2	29.49	5.33
0.4	29.65	4.64
0.6	29.80	3.12
0.8	33.76	3.06
1	32.96	2.87

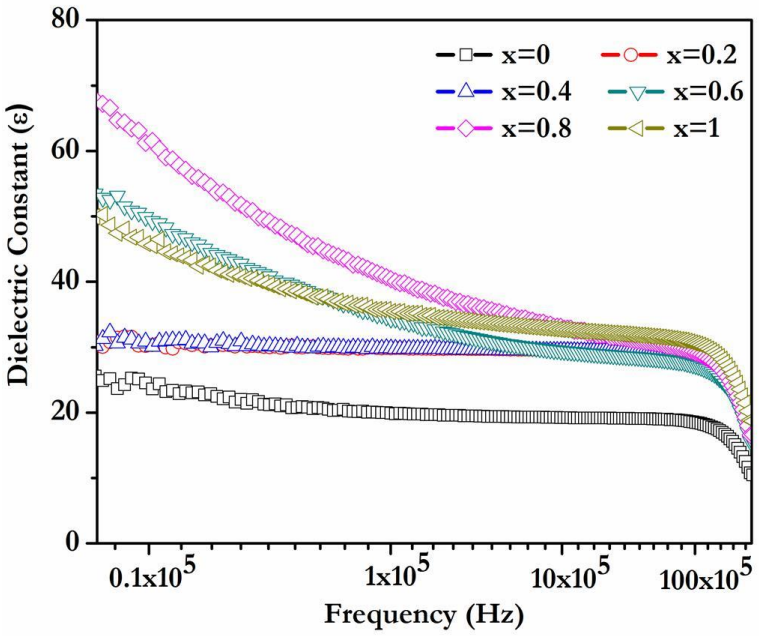

Figure 5.11 Dependence of dielectric constant with frequency.

Figure 5.11 & Figure 5.12 shows the dielectric constant (ε) and resistivity (ρ) with frequency, respectively and Table 5.6 summarizes the values at 1 MHz. As shown in Table 5.6, the values of Ɛ increase with an increase in Co contents up to x = 0.8 and then decreases with an increase of Co concentration. Frequency dependent dielectric constant are shown in Figure 5.11. It is clear from the figure that initially dielectric constant is increased at lower frequency and then it is decrease rapidly with increasing frequency. It can be explained by the theory of Maxwell-Wagner polarization and koop's model [Wagner (1913), Koop (1951), Maxwell (1982)]. At lower frequency, it contains large dielectric constant due to the dipolar and interfacial polarizations. It may easily follow the applied field and results in the large polarization. While at high frequency, the hopping of the charge may not follow the applied field. From the Table 5.6, it is observed that Co^{+2} substitution increases the dielectric constant up to x = 0.8. It is due to Co^{+2} ,which increases the hopping of electrons between Fe^{+2}- Fe^{+3} at octahedral site [Aravind*et*

al. (2016)]. Further at x = 1.0, dielectric constant is observed to decrease. Anwar and Maqsood (2014) have reported that small grain size and low concentration of polarizable ions lead to the decrease in dielectric constant. The small grains are increased the insulating grain boundaries and therefore, increase the energy barrier in hopping of electrons between Fe^{+2} and Fe^{+3} ions. The similar behavior of Co^{+2} substituion has been reported by Anwar and Maqsood (2014).

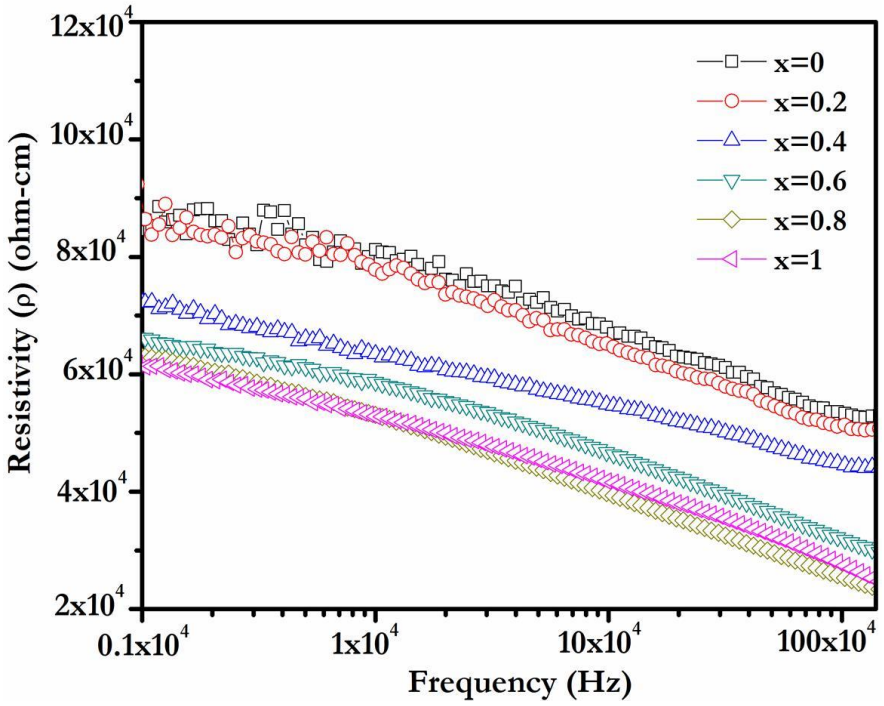

Figure 5.12 Change of AC resistivity with frequency of $SrAl_4Fe_{(8-x)}Co_xO_{19}$ ferrite with different Co contents.

Figure 5.12 shows the frequency dependency of ac resistivity (ρ) for sintered specimen and values of resistivity at 1 MHz are tabulated in the Table 5.6. It is seen that resistivity decreases almost linearly with the increase in frequency due to the inverse relationship between them. From the Figure 5.12, it is also found that the resistivity of the sample decreases with Co content in the system. It may be attributed to the increase of average grain

size with the increase of Co content in the composition. The bigger grains result in less number of grain boundaries, which act as a scattering center for the flow of electrons in the system and therefore, grain boundaries are highly resistive [Low and Sale (2002)]. The other reason may be increased in drift mobility (μ_d) with Co addition.

5.3 Summary

Co^{+2} ion substituted $SrAl_4Fe_{8-x}Co_xO_{19}$ ferrite nanoparticles are synthesized successfully by sol-gel auto combustion method. The XRD studies are revealed the formation of M-type hexagonal structure after calcining in air at 1100 ^oC for 2hrs. The grain size of the matrix is increased with the increase in the concentration of Co^{+2} ions. The magnetic properties of the prepared samples are enhanced by the partial Co inclusions. The remnant flux density is increased whereas, the coercivity and Curie temperature is decreased with the increase in cobalt concentration due to increase in grain size. Dielectric spectra shows decreasing trend of ε with respect to frequency in the studied frequency range.